ChemPubSoc Europe

DOI: 10.1002/chem.201603497

CHEMISTRY A European Journal Communication

Nanostructures

Heterostructures through Divergent Edge Reconstruction in Nitrogen-Doped Segmented Graphene Nanoribbons

Tomas Marangoni,[a] Danny Haberer,[a] Daniel J. Rizzo,[b] Ryan R. Cloke,[a] and Felix R. Fischer*[a, c, d]

Abstract: Atomically precise engineering of defined segments within individual graphene nanoribbons (GNRs) represents a key enabling technology for the development of advanced functional device architectures. Here, the bottom-up synthesis of chevron GNRs decorated with reactive functional groups derived from 9-methyl-9H-carbazole is reported. Scanning tunneling and non-contact atomic force microscopy reveal that a thermal activation of GNRs induces the rearrangement of the electron-rich carbazole into an electron-deficient phenanthridine. The selective chemical edge-reconstruction of carbazole-substituted chevron GNRs represents a practical strategy for the controlled fabrication of spatially defined GNR heterostructures from a single molecular precursor.

Lateral quantum confinement of graphene into narrow, quasi-one-dimensional graphene nanoribbons (GNRs) (width <10 nm) leads to the emergence of exotic electronic and magnetic properties.[1] The bandgap, the Fermi level, and the spin states lining the edges of GNRs can be finely tuned by varying the width, the edge structure, and the symmetry.[2] Recent advances in the bottom-up synthesis of GNRs from molecular precursors have seen new strategies to control the width,[3] the sequence, and position of heteroatom dopants along the edges (nitrogen, sulfur) and the backbone (boron) of GNRs,[4] and the rational control of the GNR symmetry (armchair GNRs and zig-zag GNRs) by the appropriate selection of molecular precursors.[5] A longstanding challenge toward the development of advanced functional devices lies in the control of the segmentation and the band alignment within individual ribbons. GNR heterostructures comprised of segments containing more than one distinctive molecular building block have thus far only been generated through an uncontrolled co-deposition strategy.[6] Therein, co-sublimation of two dissimilar but structurally compatible building blocks, featuring distinctive electronic structures, on a metal surface, followed by their random co-polymerization and subsequent cyclodehydrogenation afforded GNRs featuring an irregular number and sequence of heterojunctions along the length of the ribbon. This process is adequate for the synthesis of unique samples of GNR heterojunctions, but it provides no control over the sequence and is furthermore strictly limited to molecular building blocks that share key process parameters such as adsorption energy, phase mixing, diffusion rate, activation, polymerization, and cyclodehydrogenation temperatures.

Here, we introduce a novel bottom-up synthetic strategy founded on the intrinsic reactivity of a single molecular precursor, which allows for a late-stage functionalization of segments along a GNR. Rather than relying on the co-polymerization of two dissimilar molecular precursors, we designed a molecular building block bearing a 9-methyl-9*H*-carbazole substituent as an internal reactive moiety (**1** in Figure 1). Previous work demonstrated that the thermally induced rearrangement of 9-methyl-9*H*-carbazole at $T>500\,^{\circ}C$ on a CaO support leads to a product mixture containing both phenanthridine and carbazole.[7] Once incorporated into the edges of a fully fused GNR, the electron-rich 9-methyl-9*H*-carbazole could thus be converted into an electron-deficient phenanthridine substituent through a thermally induced ring-expansion/dehydrogenation reaction. This transformation is of particular interest in the context of rational GNR heterostructure engineering, because it would allow for a versatile and reliable strategy toward the incorporation of heterocycles with diametrically opposite inductive effects (the electron-accepting phenanthridine and electron-donating carbazole) at defined positions along the GNR backbone. We describe the synthesis of the carbazole-functionalized molecular precursor **1** and its thermally induced polymerization/cyclodehydrogenation on Au(111) in ultra-high vacuum (UHV). Scanning tunneling microscopy (STM) of thermally annealed samples reveal the characteristic pattern of chevron GNRs emerging from **1**. Bond-resolved imaging of the cyclization/dehydrogenation product using non-contact atomic force microscopy (nc-AFM) indicates that the resulting GNRs feature atomically defined heterojunctions between segments

[a] *Dr. T. Marangoni, Dr. D. Haberer, Dr. R. R. Cloke, Prof. Dr. F. R. Fischer*
Department of Chemistry, University of California Berkeley
699 Tan Hall, Berkeley, CA 94720 (U.S.A.)
E-mail: ffischer@berkeley.edu

[b] *D. J. Rizzo*
Department of Physics, University of California Berkeley
345 Birge Hall, Berkeley, CA 94720 (United States)

[c] *Prof. Dr. F. R. Fischer*
Materials Science Division, Lawrence Berkeley National Laboratory
Berkeley, CA 94720 (United States)

[d] *Prof. Dr. F. R. Fischer*
Kavli Energy NanoSciences Institute at
the University of California Berkeley and
the Lawrence Berkeley National Laboratory
Berkeley CA 94720 (United States)

Supporting information for this article can be found under http://dx.doi.org/10.1002/chem.201603497.

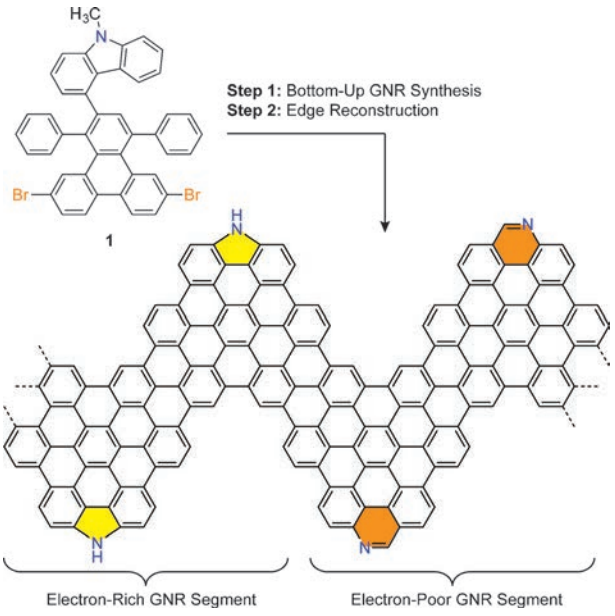

Figure 1. Schematic representation of the bottom-up synthesis of segmented nitrogen-doped chevron GNRs through an edge-reconstruction strategy. Electron-rich carbazole (yellow) and electron-deficient phenanthridine (orange) subunits along the edges emerge from a thermal rearrangement of the 9-methyl-9*H*-carbazole in building block **1**.

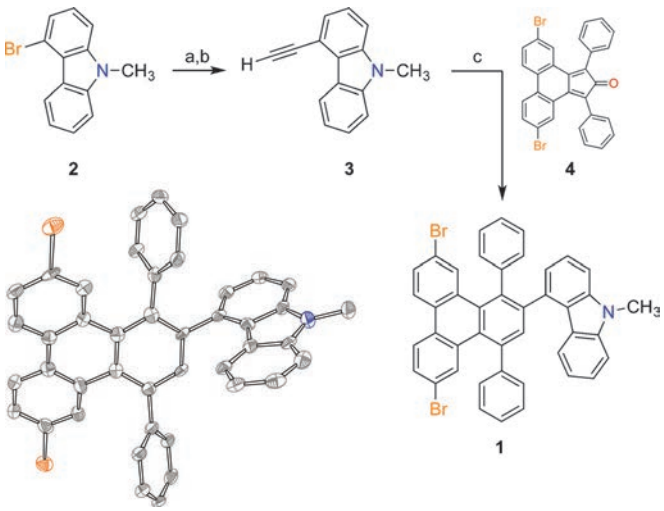

Scheme 1. Synthesis of the carbazole-substituted molecular precursor **1**. Reaction conditions: a) $[Pd(PPh_3)_4]$, CuI, TMSA, 90 °C, 24 h; b) K_2CO_3, MeOH, THF, 24 °C, 2 h, 55% (over two steps); c) **4**, *o*-xylene, 145 °C, 24 h, 32%. ORTEP representation of the X-ray crystal structure of **1**. Thermal ellipsoids are drawn at a 50% probability level. Color coding: C (gray), Br (orange), N (blue).

lined by carbazole and phenanthridine substituents. Close analysis of intermediate cyclization/dehydrogenation products indicates that the thermal rearrangement of 9-methyl-9*H*-carbazole on a Au(111) surface proceeds at $T \approx 250$ °C coinciding with the initial cyclization of **1**.

The molecular GNR precursor **1** was prepared following the synthetic pathway outlined in Scheme 1. Sonogashira–Hagihara cross-coupling of 4-bromo-9-methyl-9*H*-carbazole (**2**) with TMSA, followed by deprotection of the TMS group, yields the terminal alkyne **3** in 55% yield. Diels–Alder cycloaddition of **3** with cyclopentadienone **4** and subsequent cheletropic extrusion of CO affords the GNR precursor **1** in 32% yield. Colorless crystals of **1** suitable for X-ray diffraction were grown by slow evaporation of a saturated solution of **1** in MeCN/toluene. In the crystal structure, the 9-methyl-9*H*-carbazole substituent and the asymmetrically substituted triphenylene core adopt a dihedral angle of 86°. The packing of **1** in the crystal structure is dominated by C–H···π interactions between neighboring 9-methyl-9*H*-carbazole units (Supporting Information, Table 1SI).

Sublimation of GNR building block **1** in UHV onto a Au(111) surface maintained at 25 °C lead to a sub-monolayer coverage of self-assembled molecular islands with an apparent height of 0.45 nm as determined by LT-STM (4.5 K) (Figure 2a). Annealing of molecule-decorated Au(111) surfaces at 200 °C for 30 min induces the homolytic cleavage of the C–Br bonds. Lateral diffusion and recombination of the resulting carbon-centered diradicals through a step-growth polymerization mechanism leads to the formation of linear chains of *poly*-**1** (Supporting Information, Figure 1SI). LT-STM reveals that *poly*-**1** aggregates into parallel-aligned islands directed through favorable interactions between the carbazole substituents. Raising the annealing temperature to 250 °C induces a stepwise cyclodehydrogenation reaction that yields partially cyclized chevron GNRs (Figure 2b). LT-STM imaging indicates that the electron-rich carbazole substituents lining the periphery of *poly*-**1** readily undergo fusion with the triphenylene core at 250 °C (average height 0.17 nm; Supporting Information, Figure 2SI). The reaction of the phenyl groups lining the backbone of the polymer, however, remains incomplete. A representative sequence of commonly observed partial cyclization patterns is depicted in Figure 2d. Further annealing at 400 °C leads to an exhaustive cyclodehydrogenation and the formation of extended GNRs (Figure 2c). LT-STM reveals GNRs exhibiting the chevron topology expected from the cyclization of precursor **1**, a uniform apparent height of 0.16 nm, and an average length of 12 nm.

In an effort to unequivocally assign the structure and the substitution pattern emerging from the incorporation of 9-methyl-9*H*-carbazole along the edges of chevron GNRs, we performed sub-nanometer resolved nc-AFM imaging using a low temperature qPlus-equipped commercial Omicron LT-STM at $T = 4.5$ K. The tip of the qPlus sensor was functionalized with a single CO molecule prior to imaging the sample in constant height mode (the nc-AFM contrast in Figure 3 arises from a frequency shift of the qPlus resonator held at 23.17 kHz). Figure 3a depicts a representative nc-AFM image displaying the internal bond-resolved structure of GNRs emerging from building block **1**. The backbone of the ribbon, comprised of fully fused sp^2-hybridized carbon atoms, is reminiscent of previously fabricated chevron GNRs. A closer analysis of nc-AFM images reveals the presence of two distinctive structural motifs lining the convex protrusions of the GNRs. The 9-methyl-9*H*-carbazole substituents present in **1** undergoes a secondary thermally induced transformation, leading to the incorporation of

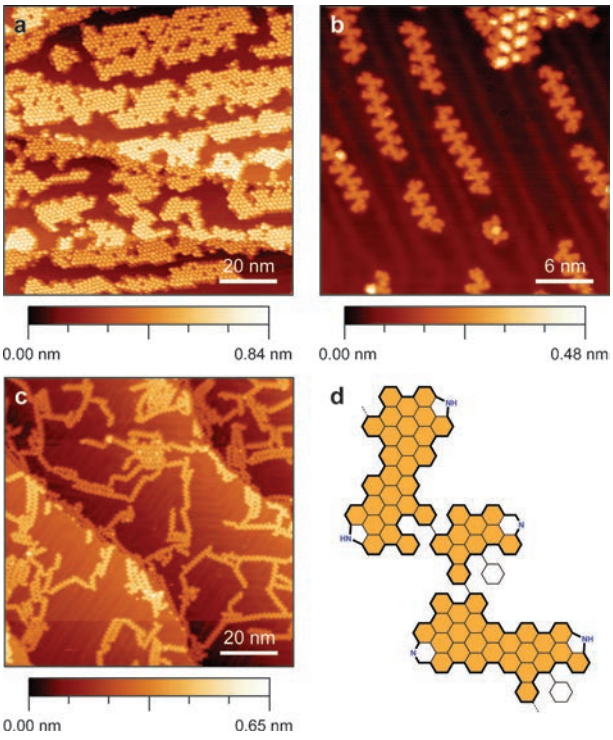

Figure 2. a) LT-STM topographic image of **1** as deposited on Au(111) ($V_s = 50$ mV, $I_t = 20$ pA, $T = 4.5$ K). b) STM image of partially cyclized *poly*-**1** obtained after annealing **1** at 250 °C on Au(111) ($V_s = 50$ mV, $I_t = 20$ pA, $T = 4.5$ K). c) Overview image of fully cyclodehydrogenated GNR heterostructures following annealing at 400 °C ($V_s = 50$ mV, $I_t = 30$ pA, $T = 4.5$ K). d) Schematic representation of partially cyclized intermediate *poly*-**1**.

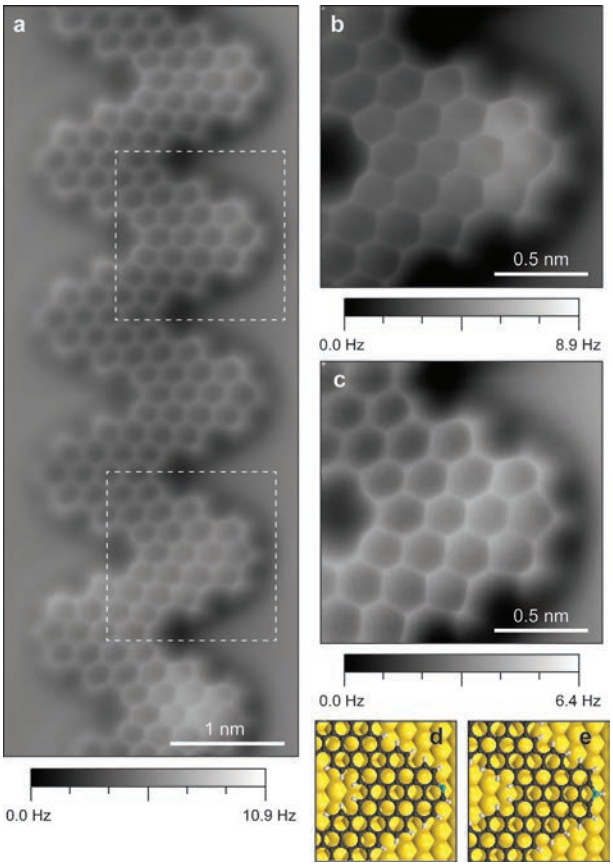

Figure 3. a) nc-AFM image (CO modified tip) of chevron GNR heterostructure on Au(111) featuring discrete segments of fused phenanthridine and carbazole groups (qPlus resonance frequency = 23.17 kHz, oscillation amplitude = 56 pm). b) nc-AFM image of phenanthridine-fused GNR segment. c) nc-AFM image of carbazole-fused GNR. d), e) Ball and stick model of phenanthridine- and carbazole-fused GNRs serves as a guide for the eye.

either a fused phenanthridine (characteristic six-membered ring in Figure 3 b, d) or a fused carbazole (characteristic five-membered ring in the Figure 3 c, e) unit in the resulting GNRs. Both structural motifs, six-membered and five-membered rings, randomly coexist in defined segments along the length of individual GNRs. The absence of defects emerging from the cleavage of the 9-methyl-9*H*-carbazole substituents in **1** or the loss of a (CH_3N) fragment indicates that the chemical transformations leading to the incorporation of phenanthridine and carbazole units are both thermodynamically and kinetically privileged.

Although the ring-expansion of 9-methyl-9*H*-carbazole to phenanthridine requires a bond-rearrangement followed by a formal loss of H_2, the nc-AFM images of carbazole units in the GNRs clearly indicate that the CH_3 group in 9-methyl-9*H*-carbazole has been cleaved and the free valence on nitrogen has been saturated by a H-atom. Cleavage of the N–CH_3 bond during the initial stages of the cyclodehydrogenation ($T \approx 250$ °C) is further corroborated by the absence of bright spots, consistent with the height profile of methyl groups, along the convex protrusions of partially cyclized GNRs in Figure 2 b (Supporting Information, Figure 2SI). Furthermore, large-area nc-AFM images of fully cyclized GNRs (Supporting Information, Figure 3SI) reveal randomly distributed structures that are consistent with the shape and triangular symmetry of surface-stabilized methyl radicals.[8]

The proposed reaction mechanism that accounts for the divergent edge-reconstruction in GNRs derived from **1**, is depicted in Scheme 2. Thermally induced homolytic cleavage of the N–CH_3 bond in the 9-methyl-9*H*-carbazole fragment leads to

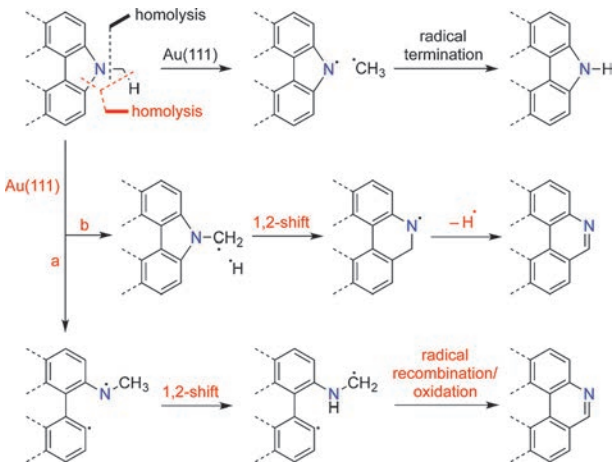

Scheme 2. Proposed mechanism for the thermally induced rearrangement of 9-methyl-9*H*-carbazole groups leading to carbazole (top) and phenanthridine (bottom) substituted chevron GNRs.

a nitrogen centered radical on the carbazole and a methyl radical stabilized through interactions with the Au(111) surface. The free valence residing on the carbazole N-atom can be saturated through radical recombination with ubiquitous surface-bound hydrogen atoms generated in the cyclodehydrogenation process. The phenanthridine substituent, instead, arises either from the homolytic cleavage of one of the two N–C_{aryl} bonds, or the homolysis of a methyl C–H bond. In the first case the radical subsequently undergoes a 1,2-H-shift from the adjacent CH_3 group to the N-atom. The dynamic rearrangement of C–H bonds in molecular radicals is facilitated through surface catalysis and has previously been reported in extended polycyclic aromatic hydrocarbons.[9] Recombination of the resulting CH_2 carbon-centered radical with the proximal Csp^2 aryl radical leads to an intermediate 5,6-dihydrophenanthridine. Oxidative dehydrogenation upon annealing the GNRs at 400 °C yields the phenanthridine substituents observed in the nc-AFM images. If the rearrangement is induced by the homolytic cleavage of a methyl C–H bond instead, a 1,2-shift leads to a ring expanded 5,6-dihydrophenanthridine radical that can lose a second hydrogen atom to give a phenanthridine group.

In summary, we report the first example of atomically precise GNR heterostructures obtained by selective reconstruction of functional groups along GNR edges. Our strategy makes use of a thermally induced site-specific ring-expansion that irreversibly converts a 9-methyl-9*H*-carbazole lining the edges of chevron GNRs into a phenanthridine group. The resulting ribbons feature fused segments lined by electron-rich carbazole and electron-deficient phenanthridine substituents. This synthetic bottom-up strategy, relying on a site-specific chemical transformation of suitable GNR substituents by an external stimulus, has the potential to provide access to intricate energy band structures that pave the way toward the development of advanced functional GNR device architectures.

Acknowledgements

Research supported by the U.S. Department of Energy (DOE), Office of Science, Basic Energy Sciences (BES), under Award #DE-SC0010409 (design, synthesis and characterization of molecules); the Center for Energy Efficient Electronics Science NSF Award 0939514 (STM and nc-AFM imaging); SPM instrument is supported by the David and Lucile Packard Foundation for Science and Engineering; Berkeley NMR Facility is supported in part by NIH grant SRR023679A; Berkeley X-ray Facility is supported in part by NIH Shared Instrumentation Grant S10-RR027172. The authors acknowledge Dr. Christian Canlas and Dr. Hasan Celik for support with NMR acquisition and Dr. Antonio DiPasquale for assistance with X-ray analysis.

Keywords: graphene · nanostructures · nc-AFM · STM · surface chemistry

[1] a) J. M. Cai, P. Ruffieux, R. Jaafar, M. Bieri, T. Braun, S. Blankenburg, M. Muoth, A. P. Seitsonen, M. Saleh, X. L. Feng, K. Müllen, R. Fasel, *Nature* **2010**, *466*, 470 – 473; b) P. Ruffieux, J. M. Cai, N. C. Plumb, L. Patthey, D. Prezzi, A. Ferretti, E. Molinari, X. L. Feng, K. Müllen, C. A. Pignedoli, R. Fasel, *ACS Nano* **2012**, *6*, 6930 – 6935; c) A. V. Rozhkov, S. Savel'ev, F. Nori, *Phys. Rev. B* **2009**, *79*, 125420; d) Y.-W. Son, M. L. Cohen, S. G. Louie, *Phys. Rev. Lett.* **2006**, *97*, 216803; e) L. Yang, C.-H. Park, Y.-W. Son, M. L. Cohen, S. G. Louie, *Phys. Rev. Lett.* **2007**, *99*, 186801; f) V. Barone, O. Hod, G. E. Scuseria, *Nano Lett.* **2006**, *6*, 2748 – 2754.

[2] a) L. Talirz, P. Ruffieux, R. Fasel, *Adv. Mater.* **2016**, *28*, 6222 – 6231; b) L. Ma, J. Wang, F. Ding, *ChemPhysChem* **2013**, *14*, 47 – 54; c) A. Narita, X.-Y. Wang, X. Feng, K. Müllen, *Chem. Soc. Rev.* **2015**, *44*, 6616 – 6643; d) X. Li, X. Wang, L. Zhang, S. Lee, H. Dai, *Science* **2008**, *319*, 1229 – 1232.

[3] a) Y.-C. Chen, D. G. de Oteyza, Z. Pedramrazi, C. Chen, F. R. Fischer, M. F. Crommie, *ACS Nano* **2013**, *7*, 6123 – 6128; b) S. Blankenburg, J. Cai, P. Ruffieux, R. Jaafar, D. Passerone, X. Feng, K. Müllen, R. Fasel, C. A. Pignedoli, *ACS Nano* **2012**, *6*, 2020 – 2025.

[4] a) R. R. Cloke, T. Marangoni, G. D. Nguyen, T. Joshi, D. J. Rizzo, C. Bronner, T. Cao, S. G. Louie, M. F. Crommie, F. R. Fischer, *J. Am. Chem. Soc.* **2015**, *137*, 8872 – 8875; b) S. Kawai, S. Saito, S. Osumi, S. Yamaguchi, A. S. Foster, P. Spijker, E. Meyer, *Nat. Commun.* **2015**, *6*, 8098; c) G. D. Nguyen, F. M. Tom, T. Cao, Z. Pedramrazi, C. Chen, D. J. Rizzo, T. Joshi, C. Bronner, Y. C. Chen, M. Favaro, S. G. Louie, F. R. Fischer, M. F. Crommie, *J. Phys. Chem. C* **2016**, *120*, 2684 – 2687; d) T. H. Vo, U. G. E. Perera, M. Shekhirev, M. Mehdi Pour, D. A. Kunkel, H. Lu, A. Gruverman, E. Sutter, M. Cotlet, D. Nykypanchuk, P. Zahl, A. Enders, A. Sinitskii, P. Sutter, *Nano Lett.* **2015**, *15*, 5770 – 5777; e) T. H. Vo, M. Shekhirev, D. A. Kunkel, F. Orange, M. J. F. Guinel, A. Enders, A. Sinitskii, *Chem. Commun.* **2014**, *50*, 4172 – 4174; f) C. Bronner, S. Stremlau, M. Gille, F. Brauße, A. Haase, S. Hecht, P. Tegeder, *Angew. Chem. Int. Ed.* **2013**, *52*, 4422 – 4425; *Angew. Chem.* **2013**, *125*, 4518 – 4521.

[5] a) P. Ruffieux, S. Y. Wang, B. Yang, C. Sanchez-Sanchez, J. Liu, T. Dienel, L. Talirz, P. Shinde, C. A. Pignedoli, D. Passerone, T. Dumslaff, X. L. Feng, K. Müllen, R. Fasel, *Nature* **2016**, *531*, 489 – 492; b) J. Liu, B.-W. Li, Y.-Z. Tan, A. Giannakopoulos, C. Sanchez-Sanchez, D. Beljonne, P. Ruffieux, R. Fasel, X. Feng, K. Müllen, *J. Am. Chem. Soc.* **2015**, *137*, 6097 – 6103.

[6] a) J. M. Cai, C. A. Pignedoli, L. Talirz, P. Ruffieux, H. Sode, L. B. Liang, V. Meunier, R. Berger, R. J. Li, X. L. Feng, K. Müllen, R. Fasel, *Nat. Nanotechnol.* **2014**, *9*, 896 – 900; b) Y.-C. Chen, T. Cao, C. Chen, Z. Pedramrazi, D. Haberer, D. G. de Oteyza, F. R. Fischer, S. G. Louie, M. F. Crommie, *Nat. Nanotechnol.* **2015**, *10*, 156 – 160.

[7] E. C. Creencia, T. Horaguchi, *J. Heterocycl. Chem.* **2006**, *43*, 1441 – 1446.

[8] B. Schuler, G. Meyer, D. Pena, O. C. Mullins, L. Gross, *J. Am. Chem. Soc.* **2015**, *137*, 9870 – 9876.

[9] a) D. G. de Oteyza, P. Gorman, Y. C. Chen, S. Wickenburg, A. Riss, D. J. Mowbray, G. Etkin, Z. Pedramrazi, H. Z. Tsai, A. Rubio, M. F. Crommie, F. R. Fischer, *Science* **2013**, *340*, 1434 – 1437; b) A. Riss, A. Perez Paz, S. Wickenburg, H.-Z. Tsai, D. G. de Oteyza, A. J. Bradley, M. M. Ugeda, P. Gorman, H. S. Jung, M. Crommie, A. Rubio, F. R. Fischer, *Nat. Chem.* **2016**, *8*, 678 – 683.

Received: July 25, 2016
Published online on August 9, 2016